CONFERENCE PRE-PRINT

THEORETICAL MODEL FOR THE EXPERIMENTALLY OBSERVED GAM'S SATELLITES

E.A. SOROKINA
National Research Centre "Kurchatov Institute"
Moscow, Russian Federation
Email: Sorokina_EA@nrcki.com

Abstract

The experimentally observed splitting of the geodesic acoustic mode (GAM) spectral peak, which is also referred as GAM's satellites formation, is explained by the nonlinear interaction of GAM with a low-frequency zonal flow in tokamak plasma. The stationary toroidal plasma rotation plays a role of the trigger, which turns on the mechanism of the modes coupling. The simplified analytical solution of the nonlinear equations is found, which describes the modulation of the GAM envelope by a low-frequency zonal flow. In the spectral pattern, this modulation is manifested as the two side-bands near the GAM frequency, the difference between which is the doubled frequency of zonal flow. The results are confirmed by the numerical integration of the full set of the nonlinear equations, which is free from the simplifying assumptions.

1. INTRODUCTION

The geodesic acoustic modes (GAMs) [1] observed in a variety of experiments with toroidal plasma are actively studied theoretically and by numerical modelling. However, there is no clear picture of their dynamics. One of the problems requiring theoretical interpretation is the observed "double–humping" of the GAM spectrum – the presence of two amplitude peaks near the theoretically calculated GAM frequency. In particular, the splitting of the GAM's peak was observed in tokamaks ASDEX Upgrade [2] and DIII-D [3]; the team of the T-10 tokamak uses the term "satellite" for this phenomenon [4].

In this paper, we exploit the theoretical model proposed in [5], which explains the presence of GAM's satellites in the spectrum of plasma electric potential oscillations by the nonlinear impact of the low-frequency zonal flow (ZF) on GAM. In the linear approximation, the low-frequency ZF, like GAM, is one of the electrostatic axisymmetric eigenmodes of toroidal plasma oscillations. The finite frequency of ZF is associated with the stationary plasma rotation [6] and vanishes in its absence. The interaction of eigenmodes with significantly different frequencies leads to the modulation of GAM's amplitude on the frequency of ZF. This effect manifests itself in the form of two side-band harmonics near the GAM standard frequency. Thus, the frequency shift between the side-band GAM peaks appears to be equal to the doubled ZF frequency that correlates with the experiment.

2. MODEL

To study the GAM-ZF interaction we use the standard system of MHD equations in electrostatic approximation. For axisymmetric perturbations, it is written as [5]

$$\frac{\partial \rho'}{\partial t} + \frac{\rho_0}{B}\mathbf{B}\cdot\nabla v_{||}' - cF\mathbf{B}\cdot\nabla\frac{\rho_0}{B^2}\frac{d\phi'}{d\Psi} = \frac{cF}{B^2}\frac{d\phi'}{d\Psi}\mathbf{B}\cdot\nabla\rho', \tag{1}$$

$$\frac{\partial p'}{\partial t} + \frac{\gamma p_0}{B}\mathbf{B}\cdot\nabla v_{||}' - cF\left(\gamma p_0\mathbf{B}\cdot\nabla\frac{1}{B^2} + \frac{1}{B^2}\mathbf{B}\cdot\nabla p_0\right)\frac{d\phi'}{d\Psi} = \frac{cF}{B^2}\frac{d\phi'}{d\Psi}\mathbf{B}\cdot\nabla p', \tag{2}$$

$$\frac{\partial v_{||}'}{\partial t} + \frac{\mathbf{B}\cdot\nabla p'}{B\rho_0} - \frac{c\Omega}{B}\mathbf{B}\cdot\nabla R^2\frac{d\phi'}{d\Psi} = \frac{cF}{B^2}\frac{d\phi'}{d\Psi}\mathbf{B}\cdot\nabla v_{||}', \tag{3}$$

$$\oint\left[p'\mathbf{B}\cdot\nabla\frac{1}{B^2} + \frac{c\rho_0|\nabla\Psi|^2}{FB^2}\frac{\partial}{\partial t}\frac{d\phi'}{d\Psi} + \frac{\Omega}{B^2}\left(\frac{\Omega\rho'}{2} + \frac{\rho_0 v_{||}'}{R}\right)\mathbf{B}\cdot\nabla R^2\right]d\theta = 0. \tag{4}$$

Equation (1) corresponds to the continuity equation, Eq. (2) is the adiabatic law with the specific heat ratio γ, Eq. (3) is the projection of the force balance equation on the direction of magnetic field $\mathbf{B} = [\nabla\Psi\times\nabla\varphi] + F(\Psi)\nabla\varphi$,

and Eq. (4) is the quasineutrality condition averaged over the magnetic surface Ψ. Standard notations for the plasma density ρ, pressure p, longitudinal velocity $v_{||}$, and electric field potential $\phi(\Psi)$, which is a function of magnetic surface, are used. Coordinate $R = R_a + r\cos\theta$ measures the distance from the geometrical centrum of a torus, θ and φ are the poloidal and toroidal angles, correspondingly. The symbol $'$ is used to mark the perturbations, while the subscript 0 is referred to stationary quantities. The CGS units are used and c is the speed of light.

We assume that in equilibrium plasma rotates in the toroidal direction with angular frequency $\Omega(\Psi)$. Due to the rotation effect, the equilibrium plasma pressure and density are stratified along the poloidal angle as [7]

$$p_0 = \bar{p}_0(r)\left(1 + \frac{r}{R_a}\gamma M^2\cos\theta\right), \quad \rho_0 = \bar{\rho}_0(r)\left(1 + \frac{r}{R_a}\frac{\gamma}{\alpha}M^2\cos\theta\right).$$

Here $\bar{p}_0, \bar{\rho}_0$ are the averaged values of equilibrium plasma pressure and density on the magnetic surface, $M = \Omega/\omega_s$ is the toroidal Mach number, and $\omega_s = \sqrt{\gamma\bar{p}_0/\bar{\rho}_0}/R_a$. An equilibrium with circular concentric magnetic surfaces of radius r ($\Psi = B_a r^2/2q$, B_a is the field on tokamak magnetic axis, q is the safety factor, and $F = B_a R_a$) is considered and the large aspect ratio approximation, $r/R_a \ll 1$, is used. Parameter α regulates the type of plasma dynamical equilibrium. In particular, $\alpha = 1$ corresponds to equilibrium with isothermal magnetic surfaces, at $\alpha = \gamma$ the entropy is a surface function, and $\alpha \to \infty$ corresponds to magnetic surfaces of constant density.

The quadratic nonlinearities are collected in the RHSs of Eqs. (1)-(3), while the higher ones are neglected due to the large aspect ratio approximation. For the same reason Eq. (4) formally remains linear.

Substituting an explicit form of $\mathbf{B}\cdot\nabla$-operator in Eqs. (1)-(4) and seeking for their solution in the form of first harmonics of the poloidal angle we come to the system of coupled ordinary differential equations:

$$\frac{\partial\rho_s}{\partial T} - \frac{v_c}{q} + A\left(2 + \frac{\gamma}{\alpha}M^2\right) = -\frac{A}{q}\rho_c, \qquad \frac{\partial\rho_c}{\partial T} + \frac{v_s}{q} = \frac{A}{q}\rho_s, \tag{5s,c}$$

$$\frac{\partial p_s}{\partial T} - \frac{v_c}{q} + A(2 + M^2) = -\frac{A}{q}p_c, \qquad \frac{\partial p_c}{\partial T} + \frac{v_s}{q} = \frac{A}{q}p_s, \tag{6s,c}$$

$$\frac{\partial v_s}{\partial T} - \frac{p_c}{q} + 2AM = -\frac{A}{q}v_c, \qquad \frac{\partial v_c}{\partial T} + \frac{p_s}{q} = \frac{A}{q}v_s, \tag{7s,c}$$

$$\frac{\partial A}{\partial T} - p_s - Mv_s - \frac{M^2}{2}\rho_s = 0. \tag{8}$$

Here the dimensionless variables $T \equiv t\omega_s$, $\rho \equiv \rho' qR_a/r\bar{\rho}_0$, $p \equiv p' qR_a/r\gamma\bar{p}_0$, $v \equiv qv'_{||}/r\omega_s$, and $A \equiv cd\phi'/d\Psi/\omega_s$ are introduced; the subscripts c and s refer to $\cos\theta$ and $\sin\theta$-harmonics.

Equations (5)-(8) constitute a closed system of equations describing the time evolution of radially-localized electrostatic axisymmetric perturbations in a conventional tokamak plasma. The numerical analysis of Eqs. (5)-(8) performed in Ref. [8] shows a variety of oscillation regimes inherent in this system. Here we consider a simplified analytical solution of Eqs. (5)-(8) implementing the iterative procedure. In a linear approximation, Eqs. (5)-(8) are reduced to the eigenmode equations for GAM and ZF. In the next approximation, we take into account the RHSs of Eqs. (5)-(8) using the linear eigenmodes in quadratic terms.

The proposed approach reduces Eqs. (5)-(8) to only three equations for the functions p_s, p_c and A. Differentiating equations (6) and (8) by time and excluding the perturbations of ρ and v, we obtain

$$\frac{\partial^2 p_s}{\partial T^2} + \frac{p_s}{q^2} + (2 + M^2)\frac{\partial A}{\partial T} = -\frac{1}{q}\left(p_c\frac{\partial A}{\partial T} + 2A\frac{\partial p_c}{\partial T}\right), \tag{9s}$$

$$\frac{\partial^2 p_c}{\partial T^2}+\frac{p_c}{q^2}-\frac{2MA}{q}=\frac{1}{q}\left(p_s\frac{\partial A}{\partial T}+2A\frac{\partial p_s}{\partial T}+(2+M^2)A^2\right), \tag{9c}$$

$$\frac{\partial^2 A}{\partial T^2}+2AM^2+A\frac{M^4}{2}\left(\frac{\gamma}{\alpha}-1\right)-\left(1+\frac{M^2}{2}\right)\frac{\partial p_s}{\partial T}-\frac{Mp_c}{q}=-MA\left(\frac{\partial p_s}{\partial T}+(2+M^2)A\right). \tag{10}$$

The solutions of linearized (with no RHSs) Eqs. (9)-(10) are the modes oscillating with constant amplitudes, $p_{c,s}=p_{c,s}^0\exp(-i\omega T)$, $A=A^0\exp(-i\omega T)$, where frequency ω is measured in units ω_s. Equations (9) determine the linear relations between the fluctuations of pressure and electric field for the considered modes

$$p_s^0=-\frac{i\omega(2+M^2)A^0}{(\omega^2-1/q^2)},\quad p_c^0=-\frac{2MA^0}{q(\omega^2-1/q^2)}, \tag{11}$$

while Eq. (10) reduces to the dispersion law with two branches [7]:

$$\omega^2=\frac{1}{2}\left\{2+\frac{1}{q^2}+4M^2+\frac{\gamma M^4}{2\alpha}\pm\sqrt{\left(2+\frac{1}{q^2}+4M^2+\frac{\gamma M^4}{2\alpha}\right)^2-\frac{\gamma-\alpha}{\alpha}\frac{2M^4}{q^2}}\right\}.$$

The higher branch corresponds to the GAM, $\omega_+^2=\omega_{GAM}^2$, while the lower one – to the ZF, $\omega_-^2=\omega_{ZF}^2$.

3. THE APPROACH OF WEAK TURBULENCE

To proceed the further analysis, we decompose the perturbations of plasma pressure and electric field in the fluctuations of GAM and ZF types, namely

$$p_{c,s}=p_{c,s}^{GAM}+p_{c,s}^{ZF},\qquad A=A^{GAM}+A^{ZF}. \tag{12}$$

Here and below we neglect the self-action of the modes and consider only the nonlinear dynamics of the GAM under the influence of a "given" linear ZF eigenmode of constant amplitude: $p_{c,s}^{ZF}=p_{c,s}^{ZF0}\exp(-i\omega_{ZF}t)$, $A^{ZF}=A^{ZF0}\exp(-i\omega_{ZF}t)$. Values $p_{c,s}^{ZF0}$ and A^{ZF0} are constant and are related to each other by linear relations (11), in which $\omega=\omega_{ZF}$.

To find the nonlinear solution for the GAM, we adhere to the weak turbulence approach [9], which assumes the nonlinear interaction of eigenmodes, leading to a slow variation of their amplitudes in time. Following this ansatz, we assume that

$$p_{c,s}^{GAM}=\bar{p}_{c,s}(T)\exp(-i\omega_{GAM}T),\qquad A^{GAM}=\bar{A}(T)\exp(-i\omega_{GAM}T), \tag{13}$$

where $\bar{p}_{c,s}$ and $\bar{A}$ are the time-dependent amplitudes of the pressure and the electric field in the GAM, whereby

$$\left|\frac{\partial\bar{p}_{c,s}}{\partial T}\right|\ll\left|\omega_{GAM}\bar{p}_{c,s}\right|,\qquad \left|\frac{\partial\bar{A}}{\partial T}\right|\ll|\omega_{GAM}\bar{A}|. \tag{14}$$

Such a representation is natural to account for the interaction of modes with significantly different frequencies.

After the substitution of the ansatz (12), (13) with the ordering (14), Eqs. (9)-(10) decompose into the "fast" and the "slow" ones. The fast equations coincide with the linear equations and give the GAM eigenfrequency, ω_{GAM}. The slow equations describe the change in the GAMs amplitude under the nonlinear effects:

$$\omega_{GAM}\frac{\partial\bar{p}_s}{\partial T}+\frac{i(2+M^2)}{2}\frac{\partial\bar{A}}{\partial T}=\frac{MA^{GAM0}A^{ZF0}\exp(-i\omega_{ZF}T)}{q^2}\left(\frac{\omega_{ZF}+2\omega_{GAM}}{\omega_{GAM}^2-1/q^2}+\frac{\omega_{GAM}+2\omega_{ZF}}{\omega_{ZF}^2-1/q^2}\right), \tag{15}$$

$$\omega_{GAM}\frac{\partial\bar{A}}{\partial T}-\frac{i(2+M^2)}{4}\frac{\partial\bar{p}_s}{\partial T}=\frac{iM(2+M^2)A^{GAM0}A^{ZF0}\exp(-i\omega_{ZF}T)}{2q^2}\left(\frac{1}{\omega_{GAM}^2-1/q^2}+\frac{1}{\omega_{ZF}^2-1/q^2}\right). \tag{16}$$

To obtain Eqs. (15)-(16), we have used the linear eigenmodes and their inherent relations (11) in the RHSs of Eqs. (9)-(10). Now, excluding $\partial\bar{p}_s/\partial T$, we come to the equation, which describes the time evolution of the amplitude of GAM's electric field under the influence of ZF:

$$\frac{\partial \bar{A}}{\partial T} = i\nu A^{GAM0} A^{ZF0} \exp(-i\omega_{ZF} T), \quad \text{where} \tag{17}$$

$$\nu = \frac{M(1+M^2/2)}{q^2(2\omega_{GAM}^2 - (1+M^2/2)^2)} \left[\frac{4\omega_{GAM} + \omega_{ZF}}{\omega_{GAM}^2 - 1/q^2} + \frac{3\omega_{GAM} + 2\omega_{ZF}}{\omega_{ZF}^2 - 1/q^2} \right].$$

To get away from the imaginary in Eq. (17), let's rewrite its RHS in terms of the time derivative of A^{ZF}

$$\frac{\partial \bar{A}}{\partial T} = -\frac{\nu A^{GAM0}}{\omega_{ZF}} \frac{\partial A^{ZF}}{\partial T}.$$

Integrating it with constant A^{GAM0} and also choosing the initial phases of GAM and ZF being equal zero: $A^{GAM} = \bar{A}\cos(\omega_{GAM} T)$, $A^{ZF} = A^{ZF0}\cos(\omega_{ZF} T)$, we finally come to the expression

$$A^{GAM} = A^{GAM0} \left(1 - \eta \frac{\omega_{GAM}}{\omega_{ZF}} \cos(\omega_{ZF} T) \right) \cos(\omega_{GAM} T). \tag{18}$$

According to (18), the nonlinearity leads to amplitude modulation of GAM by a low frequency ZF. Even for the case $|\eta| \ll 1$, where $\eta = \nu A^{ZF0}/\omega_{GAM}$, the big multiplier $\omega_{GAM}/\omega_{ZF} \gg 1$ makes possible the existence of the regimes with a large depth of modulation.

The first term in Eq. (18) corresponds to the "initial" GAM, while the second one could be rewritten in the form $\sim(\cos(\omega_{GAM} + \omega_{ZF})T + \cos(\omega_{GAM} - \omega_{ZF})T)$, which clearly indicates the formation of two side-bands on the sum and on the difference of GAM and ZF frequencies.

4. GAMS SATELLITES

The results of the model are presented below for the following values: GAM linear frequency $f_{GAM} = 21$ kHz, ZF frequency $f_{ZF} = 2$ kHz, the ratio of the amplitudes of the ZF to the GAM $A^{ZF0}/A^{GAM0} = 0.6$ and $\eta = 0.3$. The electric field fluctuations of GAM and ZF linear modes are shown in Fig. 1 with red and yellow colors correspondingly. The GAM nonlinear signal calculated with use of Eq. (18) is shown on the same figure in blue. The sufficient modulation of the GAM electric field oscillation is observed with a period of ZF in a half of millisecond.

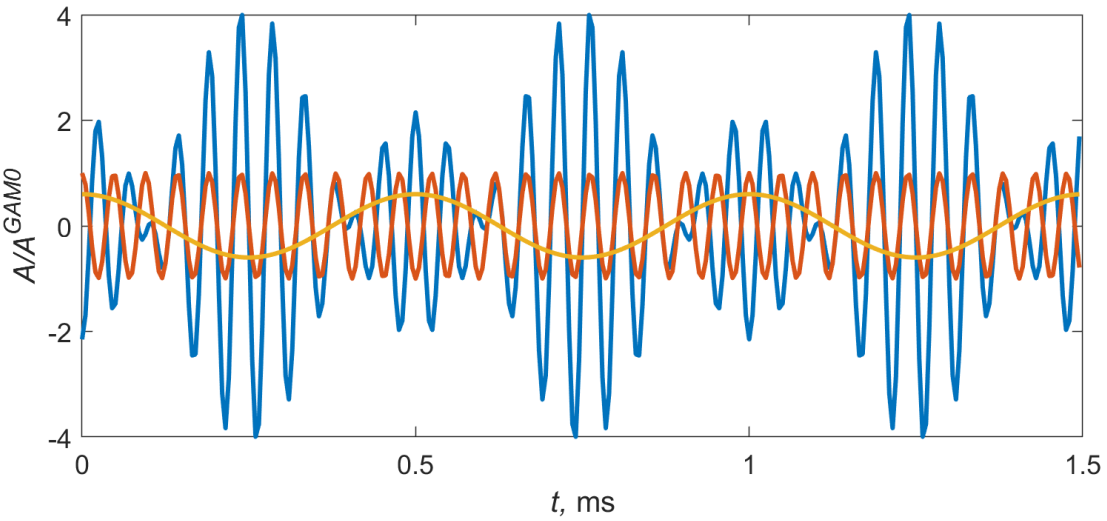

FIG. 1. Time evolution of the electric field fluctuations in liner modes of GAM (red) and ZF (yellow), and in nonlinear GAM modified by ZF (blue).

Figure 2a shows the corresponding power spectrum of $A = A^{GAM} + A^{ZF}$. The punctured circles represent the spectrum obtained as a result of Fourier analysis of an "ideal" infinite-length signal. Four frequencies are expectedly distinguished: the frequency of ZF $f_{ZF} = 2$ kHz, the GAM frequency $f_{GAM} = 21$ kHz and two side-bands at 19 and 23 kHz. On the same figure, the solid blue line corresponds to the power spectrum calculated for the signal of 1.5 ms finite length with a leakage 0.55. This simulates the conditions of real experiments always dealing with a finite signal and limited frequency resolution. Due to the low spectral resolution, the distance between the GAM and its side-bands is not well resolved that leads to an integral "two-humped" structure of the spectrum.

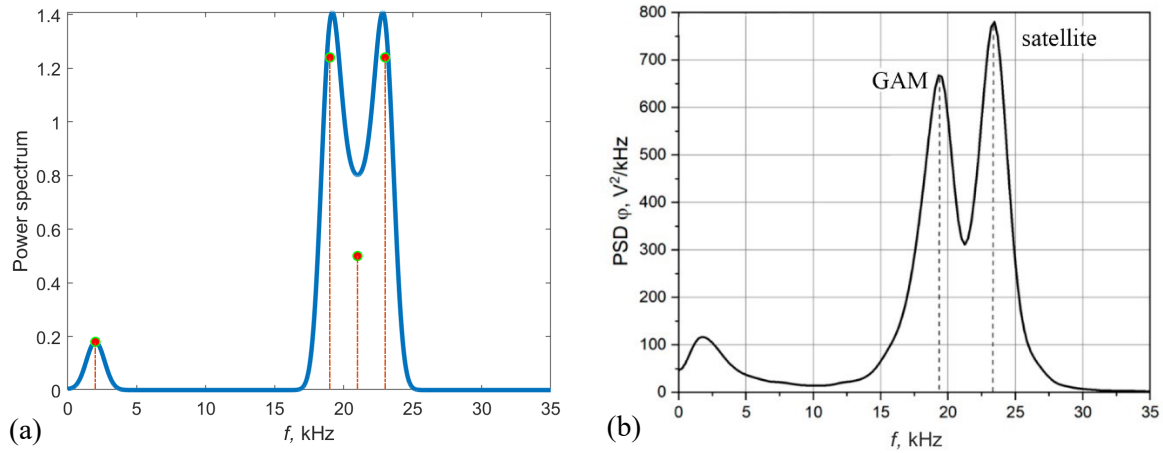

FIG. 2. Power spectrum of the electric field oscillations $A = A^{GAM} + A^{ZF}$ calculated within the framework of the nonlinear GAM-ZF model (18) at $f_{GAM}/f_{ZF} = 21/2$, $A^{ZF0}/A^{GAM0} = 0.6$, $\eta = 0.3$ (a), and spectrum of electric potential oscillations in the Ohmic stage of the T-10 tokamak discharge [10] (b). In (a) the circles correspond to the spectrum of ideal signal of infinite length, while the line – to the spectrum with finite frequency resolution. The figure (b) is reproduced by the permission of the author of Ref. [10]; the author's designations are preserved.

For comparison with the experiment, we refer to the theses [10] devoted to multicharacteristic study of the plasma electric potential fluctuations in the tokamak T-10 by means of a heavy ion beam probing. The experimentally measured power spectral density pattern typical for the Ohmic stage of the discharge is shown in Fig. 2b. It demonstrates the existence of two peaks near the GAM frequency at $f \sim 19$ kHz and $f \sim 23$ kHz. The additional peak in the region of 2 kHz is clearly observed, which, according to the proposed hypothesis, corresponds to ZF. The frequency difference of the satellites is equal to the doubled frequency of ZF. A similar spectral pattern with noticeable low-frequency activity were observed in other tokamaks, see, e.g., the measurements from the JIPP T-IIU tokamak [11].

5. NUMERICAL MODELING

To demonstrate the effect of the occurrence of GAM's satellites as a result of interaction with ZF within the "exact" model with no a priory assumption about the structure of the solution, we give examples of the numerical solutions of Eqs. (5)-(8). We specify the values of A^{GAM0} and A^{ZF0} as the initial conditions and calculate the initial values of $\{\rho,\ p,\ v\}$ using the known linear relations of these fluctuations with A. To avoid being limited by specific values of plasma parameters, we present the results below in terms of dimensionless variables, namely, the frequencies are given in units of ω_s and the time in $T_s = 2\pi/\omega_s$.

In Fig. 3, the power spectrum of the electric field fluctuations calculated for equilibrium with $\alpha = 1$ (isothermal magnetic surfaces), $M = 0.7$ (fast toroidal plasma rotation) and $q = 3$ is shown. For these values of plasma parameters, $\omega_{GAM} \approx 2.1$, $\omega_{ZF} \approx 0.05$. The quantities $A^{GAM0} = 0.3$, $A^{ZF0} = 0.1$ are used as the initial values. One can see that the general structure of the spectrum is very close to that of the simplified model. The GAM spectral pattern has a two-humped structure with the distance between the peaks equal to the doubled frequency of ZF. The amplitude of the peak related to the frequency of the standard GAM ω_{GAM} is less than that of the side-bands.

Two additional effects are clearly seen, which are not "caught" by the simplified model of GAM-ZF interaction: the appearance of secondary side-bands and the "asymmetry" of satellite peaks.

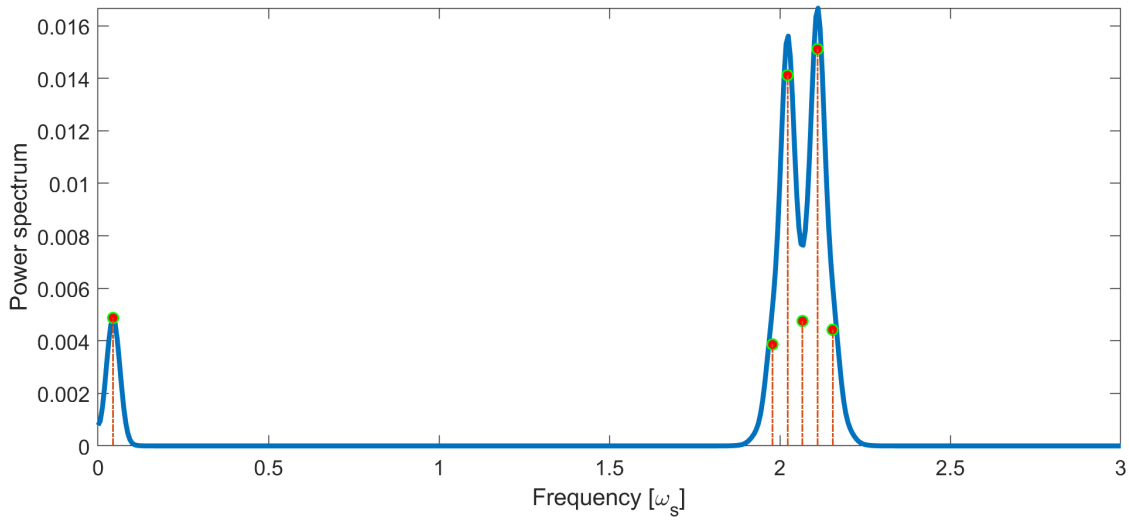

FIG. 3. Power spectrum of the electric field oscillations A calculated by the numerical integration of Eqs. (5)-(8) at $\alpha = 1, M = 0.7,\ q = 3, A^{GAM0} = 0.3, A^{ZF0} = 0.1.$ *The circles correspond to the spectrum calculated on the time interval* $568T_s$*, while the line – to the spectrum with the reduced spectral resolution.*

The results for the equilibrium with the magnetic surfaces of constant density are presented in Fig. 4. The peculiarity of this case is that the ZF is linearly unstable. Due to the nonlinearity, the amplitude of the linearly unstable ZF saturates at the early stages of the evolution and transforms into resulting oscillations of a finite frequency [12]. The further interaction of the saturated ZF mode with GAM is similar to the one for stable case.

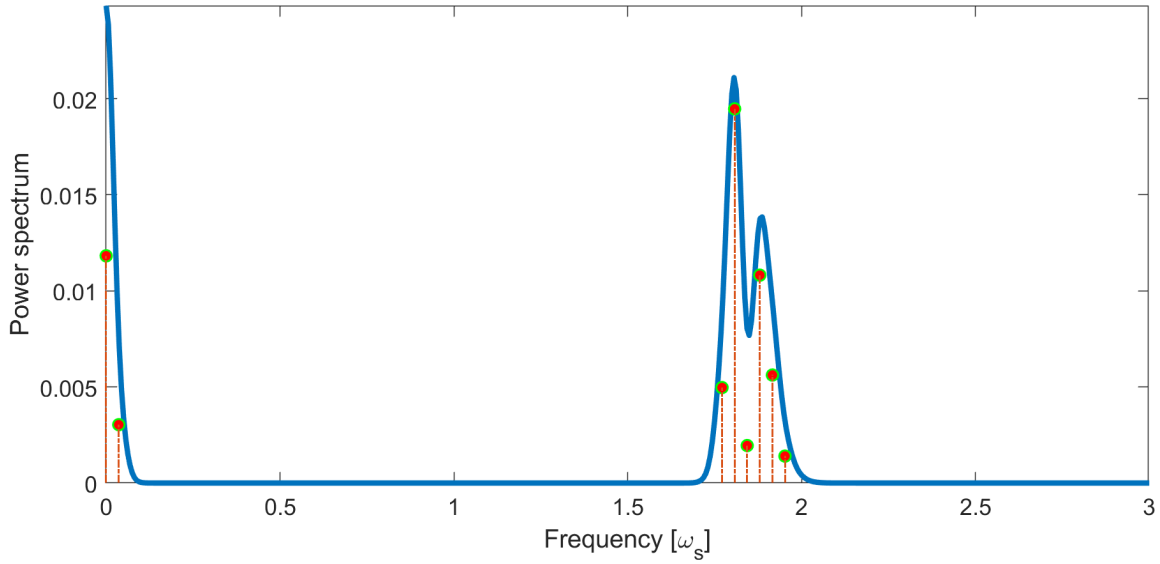

FIG. 4. Power spectrum of the electric field oscillations A calculated by the numerical integration of Eqs. (5)-(8) at $\alpha = 1000, M = 0.5,\ q = 3, A^{GAM0} = 0.3, A^{ZF0} = 0.1.$ *The circles correspond to the spectrum calculated on the time interval* $1160T_s$*, while the line – to the spectrum with the reduced spectral resolution.*

6. CONCLUSIONS

The analytical model of the nonlinear evolution of axisymmetric plasma electric potential fluctuations is proposed. The model explains the experimentally observed formation of GAMs satellites by modulation of GAM oscillations at the frequency of ZF. The analysis is based on the approach typical for the weak turbulence theory, in which a

small nonlinearity leads to a slow variation of the amplitudes of eigenmodes. The periodic change in the GAM amplitude is manifested as two side-band harmonics (satellites) with the frequencies equal to the sum and to the difference of the GAM and ZF frequencies. It is interesting that the amplitudes of the satellites can exceed the amplitude of the original GAM. Note that the solutions obtained for the same equations but by the asymptotic expansion technique cannot reproduce the experimentally observed spectral pattern [13], which indicates the irrelevance of the small amplitude assumption to the experimental conditions. The performed numerical analysis of the self-consistent GAM-ZF dynamics confirms qualitatively the discovered effect, also demonstrating a more complex spectral pattern.

ACKNOWLEDGEMENTS

This work was carried out within the state assignment of NRC “Kurchatov Institute”.

REFERENCES

[1] WINSOR, N., JOHNSON, J.L., DAWSON, J.M., Geodesic acoustic waves in hydromagnetic systems, Phys. Fluids **11** 11 (1968) 2448–2450.

[2] CONWAY, G.D., TRÖSTER, C., SCOTT, B., HALLATSCHEK, K., and ASDEX UPGRADE TEAM, Frequency scaling and localization of geodesic acoustic modes in ASDEX Upgrade, Plasma Phys. Control. Fusion **50** 5 (2008) 055009.

[3] HILLESHEIM, J.C., PEEBLES, W.A., CARTER, T.A., SCHMITZ, L., RHODES, T.L., Experimental investigation of geodesic acoustic mode spatial structure, intermittency, and interaction with turbulence in the DIII-D tokamak, Phys. Plasmas **19** 2 (2012) 022301.

[4] MELNIKOV, A.V., et al, Plasma potential and turbulence dynamics in toroidal devices (survey of T-10 and TJ-II experiments), Nucl. Fusion **51** 8 (2011) 083043.

[5] SOROKINA, E.A., Transformation of a geodesic acoustic mode in the presence of a low-frequency zonal flow in a tokamak plasma, JETP Lett. **120** 9–10 (2024) 642–649.

[6] WAHLBERG, C., Geodesic acoustic mode induced by toroidal rotation in tokamaks, Phys. Rev. Lett. **101** 11–12 (2008) 115003.

[7] HAVERKORT, J.W., DE BLANK, H.J., KOREN, B., The Brunt–Väisälä frequency of rotating tokamak plasmas, J. Comput. Phys. **231** 3 (2012) 981–1001.

[8] ILGISONIS, V.I., SOROKINA, E.A., Nonlinear self-consistent dynamics of geodesic acoustic modes and zonal flows in toroidally rotating tokamak plasmas, Proc. 30th IAEA Fusion Energy Conf. (FEC 2025), Chengdu, China, 2025, # 3268.

[9] GALEEV, A.A., SAGDEEV, R.Z., “Wave-wave interaction”, Basic Plasma Physics, North-Holland, Amsterdam (1983).

[10] DRABINSKIJ, M.A., Characteristics of geodesic acoustic mode and quasi-coherent mode of plasma oscillations in tokamak T-10 with Ohmic and microwave heating, PhD Thesis, Moscow, 2023, *in Russian*.

[11] HAMADA, Y., WATARI, T., NISHIZAWA, A., IDO T., KOJIMA, M., KAWASUMI, Y., TOI, K., and the JIPPT-IIU Group, Wavelet and Fourier analysis of zonal flows and density fluctuations in JIPP T-IIU tokamak plasmas, Plasma Phys. Control. Fusion **48** 4 (2006) S177–S191.

[12] SOROKINA, E.A., Nonlinear dynamics of linearly unstable $n = 0$ electrostatic perturbations in conventional tokamak plasmas, Plasma Phys. Rep. **51** 6 (2025) 665–684.

[13] LAKHIN, V.P., On the nonlinear interaction of geodesic acoustic modes and zonal flows in tokamaks with toroidal plasma rotation, JETP **141** 1 (2025), *in press.*